AIAA-93-1492-CP

VIBRATION LOCALIZATION IN MONO- AND BI-COUPLED BLADED DISKS — A TRANSFER MATRIX APPROACH *

Gísli Óttarsson †
Christophe Pierre ‡
Department of Mechanical Engineering and Applied Mechanics
The University of Michigan
Ann Arbor, Michigan 48109-2125

ABSTRACT

A transfer matrix approach to the analysis of the dynamics of mistuned bladed disks is presented. The study focuses on mono-coupled systems, in which each blade is coupled to its two neighboring blades, and bi-coupled systems, where each blade is coupled to its four nearest neighbors. Transfer matrices yield the free dynamics — both the characteristic free wave and the normal modes — in closed form for the tuned assemblies. Mistuned assemblies are represented by random transfer matrices and an examination of the effect of mistuning on harmonic wave propagation yields *the localization factor* — the average rate of spatial wave amplitude decay per blade — in the mono-coupled assembly. Based on a comparison of the wave propagation characteristics of the mono- and bi-coupled assemblies, important conclusions are drawn about the effect of the additional coupling coordinate on the sensitivity to mistuning and the strength of mode localization predicted by a mono-coupled analysis.

1 INTRODUCTION

A perfectly periodic structure consists of a chain of identical elements connected to one another in an identical manner. If the last element of the chain is connected to the first one, the structure is said to have cyclic symmetry. When analyzing the dynamics of *bladed-disk assemblies* one frequently postulates perfect cyclic symmetry. This is equivalent to assuming that the bladed disk is tuned, that **is,** that all blades are strictly identical and are identically mounted and uniformly spaced on a homogeneous, symmetrical disk.

All cyclic structures share the same set of modes of vibration, called *constant interblade phase angle* modes. The vibration modes are so named, because in a normal mode motion all blades vibrate with the same amplitude and the difference in phase between the motion of adjacent blades is constant throughout the blade assembly. This assumption of perfect cyclic symmetry simplifies drastically the vibration analysis of bladed disks. Instead of analyzing the structure as a whole, the equations of motion may be uncoupled and the size of the problem reduced to that of a single blade or that of a blade-disk sector. However, designers are aware of inherent differences among rotor blades, due to material and manufacturing tolerances as well as in-service degradation, a phenomenon referred to as *rotor mistuning.* While it is widely accepted that mistuning causes a reduction in the risk of flutter instability (Bendiksen, 1984), it has also been established that mistuning has a negative effect that could outweigh this benefit, by increasing forced response amplitudes: Thus mistuning may alter the results of a tuned analysis drastically (Dye and Henry, 1969; El-Bayoumy and Srinivasan, 1975; Ewins and Han, 1984). The numerous studies of the effect of mistuning on the dynamics of blade assemblies are reviewed in a survey paper by Srinivasan (1984).

One of the most important problems that plague turbomachinery rotors is the existence of rogue blades — lone blades that exhibit unexpected fatigue failure. Recently it has been suggested that rotor mistuning might be the cause of rogue blades, through a phenomenon called normal mode localization, whereby vibrations are confined to a few blades of the assembly (Valero and Bendiksen, 1986; Wei and Pierre, 1988).

The phenomenon of vibration localization may be expected to occur in any nearly periodic structure for which perfect periodicity is prevented by small irregularities. Localization, like damping, manifests itself as a spatial decay of the vibration amplitude along the structure, but for vastly different reasons. In the case of damping, energy is dissipated as vibrations are transmitted through the system, whereas in the case of localization, the energy is merely confined to a small geometric region within the structure. Localization occurs because waves propagating away from the energy source are reflected by the boundary between the slightly different subsystems making up the nearly periodic structure. The resulting confinement of energy may lead to much higher amplitudes locally than would be predicted if perfect periodicity were assumed, with possibly disastrous effects, for example in turbomachinery. The localization phenomenon has recently received wide attention in the literature and it has been shown to occur in various types of nearly periodic structures, namely blade assemblies (Valero and Bendiksen, 1986; Wei and Pierre, 1988), multi-span structures (Kissel, 1988; Hodges, 1982; Pierre 1990), and some large space structures (Cornwell and Bendiksen, 1987, Chen and Pierre, 1992).

The manner in which the substructures, or bays, which make up a (nearly) periodic structure are interconnected plays a major role in its dynamics and in the occurrence of mode localization. It is only through these connections that vibrational energy is passed between substructures. If neighboring bays are connected through several degrees of freedom the periodic structure is said to be a multi-coupled or a multi-wave structure (Brillouin, 1953; Mead,

* This work was supported by NASA Lewis Grant NAG3-1163 with Dr. G. Stefko as the technical monitor.
† Graduate Research Assistant, Student Member AIAA
‡ Associate Professor, Member **AIAA**

1975). Conversely, if neighboring bays are only connected through a single degree of freedom, the system is mono-coupled and it carries a single pair of left- and right-traveling waves.

Each bay in a (nearly) periodic system is, in general, a multi degree of freedom substructure. Coupling between blades is due to structural coupling through the disk and aerodynamic coupling through the fluid. Blades may also be connected through a shroud. Hence a blade assembly is, in general, a complex multi-coupled (nearly) cyclic structure.

If the strength of coupling between two blades in an assembly decreases rapidly with decreasing proximity, a blade might be considered to influence only a few of its close neighbors, by ignoring the effect it has on the rest of the blades. To capitalize on this assumption, a transfer matrix approach can be introduced. For example, an assembly which features only coupling between adjacent blades can be modeled efficiently with transfer matrices of dimension twice the number of coupling coordinates (Mead, 1975). Note that the number of degrees of freedom through which a blade is coupled to its neighbors may be much smaller than the actual number of degrees of freedom accounted for in the blade itself. With the transfer matrix approach the cyclic nature of the system is taken into account by realizing that the state vector describing the behavior of each blade in an N-blade system is, at any given time, periodic with period N/n, where n is some integer.

Earlier work by the authors focused on the effects of blade mistuning on the dynamics of assemblies featuring adjacent blade coupling and a single coupling coordinate, that is, on mistuned mono-coupled cyclic structures (Óttarsson and Pierre, 1993). Using a statistical approach, a measure of sensitivity to mistuning was developed, which capitalized on the existence of only one pair of waves in the mono-coupled structure. However, this methodology may have limited validity for real-life systems such as assemblies which feature coupling among all blades, through the disk or through the aerodynamics, and for which a more comprehensive model of interblade coupling may be required. The aim of the present work is to determine under which conditions, and in which manner an additional coupling coordinate among non-adjacent blades affects the dynamics of cyclic structures and their sensitivity to mistuning.

To date, little is understood regarding the mode localization phcnomcnon in multi-coupled periodic structures with mistuning. Complex interactions are known to take place among the various wave pairs but, contrary to the mono-coupled case for which a localization factor—the rate of spatial amplitude decay per bay—can be calculated for the only existing wave type, no characterization of the attenuation of the various waves and of the transfer of energy among the wave channels is yet available (here a promising effort by Kissel (1988) should be noted). Despite this lack of a theoretical foundation, it is important to assess, at least in a qualitative way, how the existence of additional wave channels affects the localization of waves as predicted by the mono-coupled analysis. Here we attempt to answer partially this question by examining the wave propagation characteristics of a bi-coupled structure in which five neighboring bays are directly coupled. The dynamics of a general such system are studied and, as an example, we introduce an extension of Dye and Henry's model of a bladed disk (1969).

The paper is organized as follows. The concept of modeling blade assemblies as multi-coupled cyclic structures is introduced and demonstrated for mono-coupled and bi-coupled systems. The theory of wave propagation in multi-coupled periodic structures is reviewed and applied to the mono- and bi-coupled systems, yielding information about frequency passbands, stopbands and—in the case of the two-wave system-complexbands. Next, it is illustrated how the use of the transfer matrix, along with a cyclicity argument, can lead to the natural frequencies and mode shapes of the tuned system. The results of the analysis of localization of waves in the mistuned mono-coupled system are then presented and validated. Using arguments based on the propagation of waves in tuned systems, the effect of adding a second coupling coordinate (between non-adjacent blades) is predicted. This prediction is supported by an examination of the modes of mistuned mono- and bi-coupled assemblies.

The primary contribution of the paper is added insight into the effect of additional wave channels on the localization of waves in mistuned cyclic structures. It is demonstrated how the lessons learned through the study of mono-coupled systems may be utilized to predict qualitatively the range of validity of the mono-coupling assumption for assemblies with non-adjacent blade coupling, without an actual in-depth study of wave propagation in mistuned multi-coupled systems.

2 MODELING BLADE ASSEMBLIES WITH TRANSFER MATRICES

Blade assemblies may be modelled as periodic structures with the additional constraint that the dynamics at the two boundaries are identical. We refer to this type of closed periodic structure as *cyclic*. The transfer matrix modeling of any periodic or cyclic structure undergoing harmonic motion requires the definition of astute vector. For the discussion we introduce the terms *buy* and *interface*. A bay is normally defined as exactly one spatial period in the periodic structure, such that only bays that are nearest neighbors are coupled. An interface is a "point" on the structure which separates two bays. To a state vector for a interface corresponds a transfer matrix that relates the states at two consecutive interfaces, or two adjacent bays. The dimension of the state vector must be twice the number of coupling coordinates at each interface, M (Mead, 1975). A state vector is most commonly defined as the coupling coordinate amplitudes at an interface and the amplitudes of the associated forces. Displacements and forces at two consecutive interfaces are thus related as

$$\begin{bmatrix} \mathbf{q} \\ \mathbf{F} \end{bmatrix}_i = \hat{\boldsymbol{T}}_i \begin{bmatrix} \mathbf{q} \\ \mathbf{F} \end{bmatrix}_{i-1} \qquad i = 1, \ldots, N.$$

where $\mathbf{q}$ and $\mathbf{F}$ each have dimension M, where M is the number of coupling coordinates and $\hat{\boldsymbol{T}}_i$ is the transfer matrix for the ith bay, which depends on the frequency of harmonic motion. If the structure is perfectly periodic then all the transfer matrices are identical, corresponding to a blade assembly that is perfectly tuned.

Alternatively we could define a state vector for a bay as the coupling coordinate amplitudes at both ends of the bay. Then

$$\mathbf{u}_i = \boldsymbol{T}_i \mathbf{u}_{i-1} \qquad i = 1, \ldots, N \tag{2}$$

where $\mathbf{u}_i = [\mathbf{q}_{i+1}, \mathbf{q}_i]^T$ has dimension $2M$, *i.e.*, twice the number of coupling coordinates. Note that because of cyclicity $\mathbf{q}_{N+1} = \mathbf{q}_1$ and $\mathbf{q}_N = \mathbf{q}_0$. This paper is based on the latter approach. It is noteworthy that the actual number of degrees of freedom of each bay, P, may be larger (possibly much larger) than the number of coordinates, M, through which it is coupled to the other bays in the assembly. It is M that determines the dimension of the transfer matrix.

Equation (2) does not account for motion-independent external forces acting on the system and hence only the free dynamics are

considered. Furthermore, only real-valued problems shall be considered, thus ignoring damping and aerodynamic effects.

2.1 The Mono-Coupled Assembly

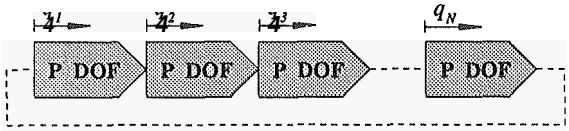

Fig. 1 A general N-bay nearly cyclic assembly with P degrees of freedom per bay, one of which couples adjacent bays.

In the case of a single coupling coordinate, $M = 1$, Eq. *(2)* is two dimensional and becomes

$$\begin{bmatrix} q_{i+1} \\ q_i \end{bmatrix} = \boldsymbol{T}_i \begin{bmatrix} q_i \\ q_{i-1} \end{bmatrix} \qquad i = 1, \ldots, N \tag{3}$$

Thus two equations that relate the coupling coordinates q_{i+1}, q_i and q_{i-1} are required. One is the equation of motion of the coupling degree of freedom of bay i:

$$-q_{i+1} + \beta_i(\omega) q_i - q_{i-1} = 0, \qquad \beta_i(\omega) \in \mathbb{R}, \tag{4}$$

Equation **(4)** does not account for dissipation since $\beta_i(\omega)$ is assumed to be real valued. The subscript i on β implies that the bays of the assembly are not identical. In the case of a tuned assembly we have $\beta_i \equiv \beta_o$ for all bays. Furthermore, Eq. **(4)** makes certain assumptions about the nature of the mistuning the details of which are beyond the scope of this paper (see (Óttarsson and Pierre, ***1993)).*** The second equation required for Eq. **(3)** is simply the identity $q_i = q_i$. Hence, each bay of a cyclic mono-coupled structure is described by a transfer matrix representation of the form

$$\begin{bmatrix} q_{i+1} \\ q_i \end{bmatrix} = \begin{bmatrix} \beta(\delta_i) & -1 \\ 1 & 0 \end{bmatrix} \begin{bmatrix} q_i \\ q_{i-1} \end{bmatrix} = \boldsymbol{T}_i \begin{bmatrix} q_i \\ q_{i-1} \end{bmatrix}, \; i = 1, \ldots, N. \tag{5}$$

where δ_i is the small deviation (order ε or smaller) of some system parameter from its average value, defining the mistuning for the i^{th} bay. This is a random variable of mean zero. In the notation, the frequency dependence of β has been dropped for clarity.

Example

Let us illustrate the above with an example. Consider the mono-coupled blade assembly with two degrees of freedom per bay shown in Fig. 2. Dye and Henry ***(1969)*** were among the first to propose this blade assembly model and it has been used subsequently both for blade assemblies (Bendiksen, ***1984)*** and for large space reflectors (Cornwell and Bendiksen, ***1987).*** This system will be utilized for demonstrative purposes for the remainder of the paper. In Fig. 2, q_i^b represents the single-mode motion of the blade and q_i^d accounts for the motion of the disk at the blade root. Corresponding to q_i^b are the blade (modal) mass m_b and (modal) stiffness k_b^i. The mass m_d simulates the effective mass of the blade root and the corresponding section of the disk. The stiffness k_d represents the stiffness of the rotor disk, whereas k_c provides disk coupling between neighboring blades. It is assumed that all bays have identical masses m_b and m_d and stiffnesses k_d and k_c, and that only the stiffness k_b^i may differ from one bay to the next. This reduces complexity and provides an adequate means of mistuning the natural frequencies of the individual bays. The average value of the blade stiffness is k_b, which corresponds to the stiffness in a tuned assembly.

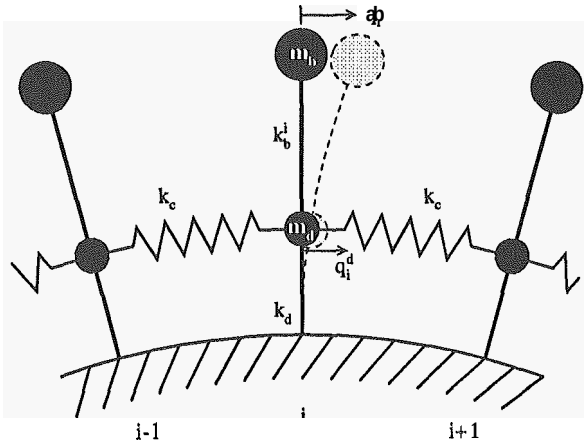

Fig. 2 The i^{th} blade in an N-blade assembly with one blade coordinate and one disk coordinate per bay is shown with its two coupled neighboring blades.

We now proceed to formulate a transfer matrix representation of the system in Fig. 2. Bay i is defined as the i^{th} blade-disk element, including the spring connecting it to blade $(i+1)$. This yields the equations of motion

$$m_b \ddot{q}_i^b + k_b^i \left(q_i^b - q_i^d \right) = 0, \tag{6}$$

$$k_c \left(q_i^d - q_{i-1}^d \right) + k_c \left(q_i^d - q_{i+1}^d \right) + k_d q_i^d + k_b^i \left(q_i^d - q_i^b \right) + m_d \ddot{q}_i^d = 0, \tag{7}$$

We introduce the small mistuning of the blade stiffness

$$k_b^i = k_b (1 + \delta_i^b) \tag{8}$$

where δ_i^b is a random variable with zero mean and standard deviation s_b. Assuming harmonic motion, $\ddot{q}_i^b = -\omega^2 q_i^b$, Eq. *(6)* may be rearranged as

$$q_i^d = \left(1 - \frac{m_b \omega^2}{k_b^i} \right) q_i^b = \left(1 - \frac{\bar{\omega}^2}{(1 + \delta_i^b)} \right) q_i^b, \tag{9}$$

where

$$\bar{\omega}^2 = \frac{m_b \omega^2}{k_b} \tag{10}$$

is a dimensionless frequency. Equation (9) is now used to eliminate the blade coordinates from Eq. (7), which becomes,

$$q_{i+1}^d = \beta(\delta_i^b) q_i^d - q_{i-1}^d \tag{11}$$

where

$$\beta(\delta_i^b) = 2 + \frac{\bar{k}_d}{\bar{k}_c} - \frac{\bar{\omega}^2 (1 + \delta_i^b)}{\bar{k}_c (1 + \delta_i^b - \bar{\omega}^2)} - \frac{\bar{m} \bar{\omega}^2}{\bar{k}_c} \tag{12}$$

and we have introduced the dimensionless parameters

$$\bar{k}_d = \frac{k_d}{k_b} \qquad \bar{k}_c = \frac{k_c}{k_b} \qquad \bar{m} = \frac{m_d}{m_b}. \tag{13}$$

This is the form required for Eq. (5). In the tuned assembly Eq. (12) simplifies to

$$\beta_o = 2 + \frac{\bar{k}_d}{\bar{k}_c} - \frac{\bar{\omega}^2}{\bar{k}_c(1-\bar{\omega}^2)} - \frac{\bar{m}\bar{\omega}^2}{\bar{k}_c}. \tag{14}$$

2.2 The Bi-Coupled Assembly

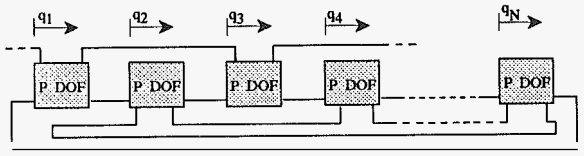

Fig. 3 A general N site cyclic assembly with P degrees of freedom per site, one of which is coupled to two adjacent sites *on each side.*

We approach bi-coupled systems ($M = 2$) through the special case of five coupled bays as depicted in Fig. 3. This definition of a bay does not conform to our earlier requirement that only neighboring bays be coupled but later we demonstrate how this case of coupled non-adjacent bays can be related to the case in which only neighboring bays are coupled. A transfer matrix representation of a system where each bay is coupled to its four nearest neighbors is

$$\begin{bmatrix} q_{i+2} \\ q_{i+1} \\ q_i \end{bmatrix} = \begin{bmatrix} -\alpha & p & -\alpha & -1 \\ 1 & 0 & 0 & 0 \\ 0 & 1 & 0 & 0 \end{bmatrix} \begin{bmatrix} q_{i+1} \\ q_i \\ q_{i-1} \\ q_{i-2} \end{bmatrix}. \tag{15}$$

The first row represents the equation of motion of the coupling coordinates of the ith bay and the remaining rows are trivial identities. The analysis of the additional degrees of freedom of each bay is performed through equations of motion which are local to the bay. Were this system to be described by a circulant system matrix (Davis, 1979), p and $-\alpha$ would be, respectively, the diagonal and the super/sub-diagonal elements of the circulant system matrix, with -1 appearing on the second off-diagonals. This would yield the system matrix $\mathbf{circ}[\beta, -\alpha, -1, 0, \ldots, 0, -1, -\alpha]$.

Example

Dye and Henry's model of a two-degree of freedom per site assembly may be easily extended to include an extra coupling spring of stiffness k_{c2}, as illustrated in Fig. 4. The disk degree of freedom at site i is now connected not only to sites $i-1$ and $i+1$, but to sites $i-2$ and $i+2$ as well. We distinguish between the stiffnesses of the two coupling springs k_{c1} and k_{c2}, so that a parametric study may reflect the effect this additional coupling parameter.

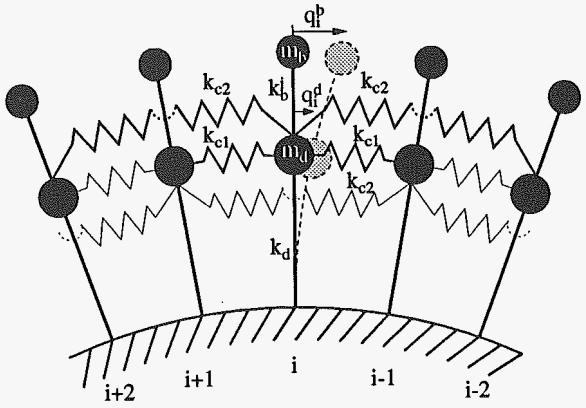

Fig. 4 A blade assembly with one disk-degree of freedom and one blade-degree of freedom per site is shown with four of its coupled neighboring blades

The equations of motion for bay i are

$$m_b \ddot{q}_i^b + k_b^i\left(q_i^b - q_i^d\right) = 0, \tag{16}$$

which is identical to Eq. (6) for the mono-coupled system. The blade stiffness mistuning is introduced as in Eq. (8) for the mono-coupled system. For the disk degree of freedom, one has

$$\begin{aligned} k_{c1}\left(2q_i^d - q_{i-1}^d - q_{i+1}^d\right) + k_{c2}\left(2q_i^d - q_{i-2}^d - q_{i+2}^d\right) \\ + k_d q_i^d + k_b^i\left(q_i^d - q_i^b\right) + m_d \ddot{q}_i^d = 0. \end{aligned} \tag{17}$$

In the case of harmonic motion, Eq. (16) may be rearranged as in Eq. (9). Using Eq. (9) to eliminate the blade coordinates from Eq. (17) yields

$$q_{i+2}^d = -\alpha q_{i+1}^d + \beta(\delta_i^b) q_i^d - \alpha q_{i-1}^d - q_{i-2}^d \tag{18}$$

corresponding to Eq. (15), where

$$\beta(\delta_i^b) = 2 + 2\frac{\bar{k}_{c1}}{\bar{k}_{c2}} + \frac{\bar{k}_d}{\bar{k}_{c2}} - \frac{\bar{\omega}^2(1+\delta_i^b)}{(1+\delta_i^b - \bar{\omega}^2)\bar{k}_{c2}} - \frac{\bar{m}\bar{\omega}^2}{\bar{k}_{c2}} \tag{19}$$

$$\alpha = \frac{\bar{k}_{c1}}{\bar{k}_{c2}} \tag{20}$$

and the additional dimensionless parameters have been introduced:

$$\bar{k}_{c1} = \frac{k_{c1}}{k_b} \qquad \bar{k}_{c2} = \frac{k_{c2}}{k_b}$$

In the tuned case, $\delta_i^b = 0$, we have

$$\beta_o = 2 + 2\frac{\bar{k}_{c1}}{\bar{k}_{c2}} + \frac{\bar{k}_d}{\bar{k}_{c2}} - \frac{\bar{\omega}^2}{(1-\bar{\omega}^2)\bar{k}_{c2}} - \frac{\bar{m}\bar{\omega}^2}{\bar{k}_{c2}}. \qquad (21)$$

2.3 Multi-Coupled Neighbors vs. Multiple Site Coupling

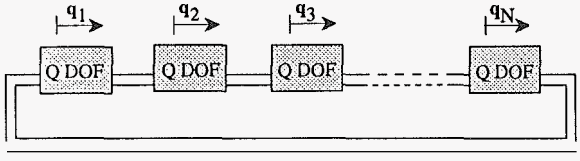

Fig. 5 A general N-bay cyclic assembly with Q degrees of freedom per bay, *two* of which are coupled to *one* adjacent bay *on each side.*

The treatment of multi-wave periodic systems usually focuses on systems where only neighboring bays are coupled through multiple coordinates, as shown in Fig. **5.** For those familiar with the work of Mead (1975), it is interesting to study the relationship between such a system and the one formulated in the previous section, which featured coupled non-adjacent bays. The form required for the transfer matrix representation of the multi-coupled system depicted in Fig. 5 is

$$\begin{bmatrix} \mathbf{q}_{i+1} \\ \mathbf{q}_i \end{bmatrix} = \begin{bmatrix} \boldsymbol{B} & -\boldsymbol{A} \\ \boldsymbol{I} & \boldsymbol{O} \end{bmatrix} \begin{bmatrix} \mathbf{q}_i \\ \mathbf{q}_{i-1} \end{bmatrix} = \boldsymbol{T} \begin{bmatrix} \mathbf{q}_i \\ \mathbf{q}_{i-1} \end{bmatrix} \qquad (22)$$

where $\mathbf{q}_i$ **is** the vector of coupling coordinate amplitudes at bay i. The block **Z** in the matrix $\boldsymbol{T}$ denotes the identity matrix and $\boldsymbol{0}$ is a block of zeros. Plainly, the system in the preceding section, shown in Fig. 3, may be modified to this form by regarding two adjacent bays as being one bay of the system shown in Fig. 5.

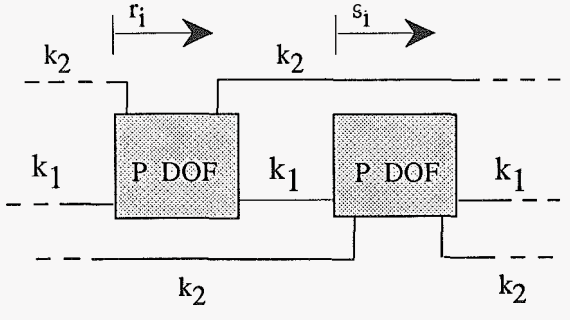

Fig. 6 An aggregate bay of the model in Fig. 3, chosen so that only neighboring substructures are coupled

This aggregate bay, which possesses $Q = 2P$ degrees of freedom, is depicted in Fig. 6. The corresponding form of the aggregate transfer matrix is obtained by multiplying two adjacent individual transfer matrices defined in Eq. (15). This yields

$$\begin{bmatrix} \mathbf{q}_{i+1} \\ \mathbf{q}_i \end{bmatrix} = \left[\begin{array}{cccc|cccc} -\mathrm{ff} & p & -\mathrm{ff} & -1 & -\mathrm{ff} & p & -\mathrm{ff} & -1 \\ 1 & 0 & 0 & 0 & 1 & 0 & 0 & 0 \\ 0 & 1 & 0 & 0 & 0 & 1 & 0 & 0 \\ 0 & 0 & 1 & 0 & 0 & 0 & 1 & 0 \end{array}\right] \begin{bmatrix} \mathbf{q}_i \\ \mathbf{q}_{i-1} \end{bmatrix}$$

$$= \begin{bmatrix} \alpha^2 - \beta & -\alpha\beta - \alpha & \alpha^2 - 1 & \alpha \\ -\alpha & \beta & -\alpha & -1 \\ 1 & 0 & 0 & 0 \\ 0 & 1 & 0 & 0 \end{bmatrix} \begin{bmatrix} \mathbf{q}_i \\ \mathbf{q}_{i-1} \end{bmatrix}$$

$$= \begin{bmatrix} \boldsymbol{B} & -\boldsymbol{A} \\ \boldsymbol{I} & \boldsymbol{O} \end{bmatrix} \begin{bmatrix} \mathbf{q}_i \\ \mathbf{q}_{i-1} \end{bmatrix} \qquad (23)$$

where

$$\mathbf{q}_i = \begin{bmatrix} r_i \\ s_i \end{bmatrix} \qquad (24)$$

The more classical representation of periodic structures in terms of coupled adjacent bays is thus easily achieved from the non-adjacent coupling formulation by a simple permutation of the state vector coordinates and the squaring of the associated transfer matrix.

3 WAVE PROPAGATION IN PERFECTLY CYCLIC STRUCTURES

We examine the propagation of waves in a general infinite periodic structure whose dynamics are governed by Eq. *(2).* It has long been known that energy-carrying motions in periodic structures only occur in isolated frequency ranges known as *passbands.* Outside the passbands, only attenuated standing waves or complex waves can take place (Mead, 1975). **A** physical understanding of these wave-propagation characteristics is achievable through the diagonalization of Eq. *(2).* This requires the solution of the eigenvalue problem:

$$\mathbf{u}_i = \boldsymbol{T}_o \mathbf{u}_{i-1} = \lambda \mathbf{u}_{i-1}, \qquad (25)$$

where $\boldsymbol{T}_o$ is the transfer matrix of a tuned assembly. Equation (25) yields the eigenvalues and eigenvectors of $\boldsymbol{T}_o$. Its significance is as follows. The eigenvectors of $\boldsymbol{T}_o$ define wave-modes, or characteristic waves, which propagate along the structure in such a way that the state-vector, $\mathbf{u}_i$, is multiplied by a complex scalar, λ, as the wave passes through each bay. The independent wave-modes define the preferred means of free wave propagation along the periodic assembly — much like normal modes are the preferred form of free vibration of a structure. The normal modes form a basis for all vibration shapes in a structure. Similarly, all possible waveforms in a structure may be written as a linear combination of wave-modes.

Eigenvalues appear in reciprocal pairs, Λ and λ^{-1}, that are either real or complex (Mead, 1975). To each eigenvalue pair thus correspond two waves which are equivalent except for their direction of travel. The eigenvalue that has modulus greater than 1 **is** associated with a wave-mode traveling and/or attenuating in the direction of decreasing bay number. We shall refer to this as the left or counterclockwise direction.

Since the dimension of the transfer matrix is twice the number of coupling coordinates between bays, the number of left- and right-traveling wave pairs equals the number of coupling coordinates for the assembly. **A** transformation between physical coordinates and wave coordinates is defined by the matrix $\boldsymbol{X}$ which has as its columns the eigenvectors of $\boldsymbol{T}_o$. The similarity transformation of $\boldsymbol{T}_o$ into wave coordinates thus yields a diagonal *wave transfer matrix* $\boldsymbol{W}_o$, as

$$\begin{bmatrix} \mathbf{L} \\ \mathbf{R} \end{bmatrix}_{i+1} = \boldsymbol{W}_o \begin{bmatrix} \mathbf{L} \\ \mathbf{R} \end{bmatrix}_i = \boldsymbol{X}^{-1} \boldsymbol{T}_o \boldsymbol{X} \begin{bmatrix} \mathbf{L} \\ \mathbf{R} \end{bmatrix}_i = \begin{bmatrix} \Lambda & 0 \\ 0 & \Lambda^{-1} \end{bmatrix} \begin{bmatrix} \mathbf{L} \\ \mathbf{R} \end{bmatrix}_i \qquad (26)$$

where **R** and **L** are vectors of right- and left-traveling wave coordinate amplitudes. **A** is a diagonal matrix of eigenvalues with modulus greater than or equal to 1.

For a given eigenvalue λ_i in **A** ($i = 1,\ldots,M$), let $\lambda_i = e_i^{\mu}$ define the complex *propagation constant*, μ_i, with $\mu_i = \gamma_i + j\sigma_i$. The corresponding reciprocal eigenvalue defines the propagation constant of the right-traveling wave, $-pi$. Here γ_i, the real part of the propagation constant, is the rate of exponential attenuation of the wave amplitude L_i from one bay to the next. The imaginary part, σ_i, is the *interblade phase angle*, the difference in phase between the motion of adjacent bays. In the literature dealing with wave propagation in periodic systems (Mead, 1975), the interblade phase angle is usually called the *wave number*. The propagation constants contains all the information about the frequency-dependent propagation of waves through the assembly. For each eigenvalue in **A** the following cases can be distinguished depending on the frequency:

- $\lambda_i \in \mathbf{R}$: For the left-traveling wave $\gamma_i > 0$, leading to attenuation. **Also,** adjacent bays are vibrating either in phase or out of phase, $\sigma_i = 0$ or $\sigma_i = \pi$, which implies that these are standing waves. These frequency ranges define *stopbands.*
- $\forall i \in \mathbb{C}$, $\lambda_i \notin \mathbb{R}$, $|\lambda_i| = 1$: In this case $\gamma_i = 0$ and no attenuation occurs. These frequencies define *apassband* in which the left- and right-going waves travel without attenuation.
- $\lambda_i \in \mathbb{C}$, $\lambda_i \notin \mathbb{R}$, $|\lambda_i| \neq 1$: For the left-traveling wave $\mu_i = \gamma_i + j\sigma_i$ with $\gamma_i > 0$ and $\sigma_i \neq 0$ or n; hence the wave travels *with* attenuation. The corresponding reciprocal eigenvalue characterizes the right-traveling wave with propagation constant $-\mu_i$. In this case the eigenvalues λ_i and λ_i^{-1} are not complex conjugate. Therefore there must be companion pair of left- and right-traveling waves with propagation constants $\gamma_i - j\sigma_i$ and $-\gamma_i + j\sigma_i$, respectively. We refer to these waves as *complex waves* and to the associated frequency ranges as complexbands. In order for them to exist there must be at least four eigenvalues, that is, at least two coupling coordinates: hence complex waves cannot occur in a mono-coupled system. Since the two left-going (and the two right-going) waves are complex conjugates, they actually represent one wave shape. Physically, the two pairs of waves merge into one in a complexband.

3.1 The Mono-Coupled Assembly

For the tuned mono-coupled system described by **Eq.** (5) the eigenvalues of the two by two transfer matrix are

$$\lambda, \lambda^{-1} = \frac{\beta_o}{2} \pm \sqrt{\left(\frac{\beta_o}{2}\right)^2 - 1}, \qquad \lambda \in \mathbb{C}, \beta_o \in \mathbb{R}, \quad (27)$$

We choose the convention that λ has modulus greater than or equal to one. The wave-modes appear as the eigenvectors, $[1, \lambda^{-1}]^T$ and $[1, \lambda]^T$, corresponding to the eigenvalues λ and λ^{-1} respectively. The two wave-modes could also be written as $[\lambda, 1]^T$ and $[1, \lambda]^T$, which shows that they are equivalent except for their direction of travel. This is supported by the symmetry of the problem to clockwise or counterclockwise numbering of the bays.

The eigenvectors of $\boldsymbol{T}_o$ are arranged defines the transformation

$$\begin{bmatrix} q_i \\ q_{i-1} \end{bmatrix} = X \begin{bmatrix} L \\ R \end{bmatrix}_i, \qquad X = \begin{bmatrix} 1 & 1 \\ \lambda^{-1} & \lambda \end{bmatrix}, \quad (28)$$

from physical coordinates to left- and right-traveling wave coordinates at bay i, corresponding to the wave-mode basis. The displacement transfer matrix $\boldsymbol{T}_o$ is thus transformed into the diagonal wave transfer matrix,

$$\begin{bmatrix} L \\ R \end{bmatrix}_{i+1} = W_o \begin{bmatrix} L \\ R \end{bmatrix}_i = \begin{bmatrix} \lambda & 0 \\ 0 & \lambda^{-1} \end{bmatrix} \begin{bmatrix} L \\ R \end{bmatrix}_i. \quad (29)$$

For this mono-coupled assembly there exists a single pair of characteristic waves. Frequency passbands and stopbands are arranged as follows:

- $|\beta_o(\omega)| < 2$: These frequencies define a *passband* in which waves travel without attenuation. From the real part of **Eq.** (27), the interblade phase angle is related to frequency by the dispersion relation:

$$2\cos a = \beta_o(\bar{\omega}), \qquad 0 < \sigma < \pi. \quad (30)$$

  For a given value of a, Eq. (30) has as many frequency solutions as there are degrees of freedom in each bay (Mead, 1975). Hence, the number of passbands equals the number of degrees of freedom in each bay, **P**. The frequencies at which $a = \pi/2$ will be referred to as *midband frequencies.* Note that the midband frequency is not necessarily located close to the mean frequency in the passband.
- $|\beta_o(\omega)| > 2$: These frequency ranges define *stopbands.*
- $|\beta_o(\omega)| = 2$: This gives $\gamma = 0$ and $\sigma = 0$ or $a = n$, and defines the bounding frequencies or the passbandstopband edges.

Example

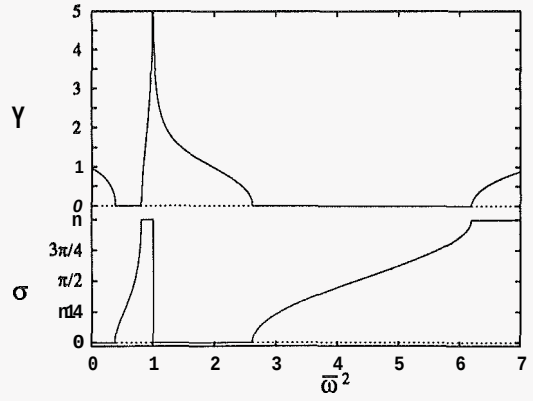

Fig. 7 The passband/stopband structure of the assembly in Fig. 2, for $\bar{k}_c = \bar{k}_d = \bar{m} = 1$ (tuned case). Note the two distinct passbands, where $\gamma = 0$. Also note a singularity at $\bar{\omega} = 1$, corresponding to the natural frequency of a cantilevered blade.

Figure 7 depicts the passband/stopband structure for the assembly in Fig. 2 **for** one set of parameter values. The rate of exponential attenuation, γ, and the interblade phase angle, σ, are displayed **as** a function of the dimensionless frequency. **As** predicted above, two frequency passbands are observed, corresponding to the two degrees of freedom per bay. In the passbands $\gamma = 0$ and unattenuated propagation of waves occurs. The wave travel is evidenced by the change of phase, $0 < a < n$, from bay to bay. The other regions are stopbands, $\gamma \neq 0$, where standing waves decay exponentially and neighboring bays are either vibrating in phase or out of phase.

A special feature for this structure is the infinite attenuation observed at $\bar{\omega} = 1$, that is, at $\omega^2 = \$$. We explain this behavior by pointing out that this is the natural frequency of a blade cantilevered at its root, hence at this frequency $q_i^d = 0$. Equation (9) confirms this. If the disk deflection equals zero, energy cannot be transmitted along the bays, hence the infinite attenuation of the waves.

3.2 The Bi-Coupled Assembly

In the tuned case the eigenvalues of the transfer matrix in Eq. **(15)** are solutions of the characteristic equation

$$\lambda^4 + \alpha\lambda^3 - \beta_o\lambda^2 + \alpha\lambda + 1 = 0 \tag{31}$$

where β_o is for the tuned system. Equation **(31)** simplifies to

$$\left[\lambda^2 + \frac{1}{2}(\alpha+\kappa)\lambda + 1\right]\left[\lambda^2 + \frac{1}{2}(\alpha-\kappa)\lambda + 1\right] = 0 \tag{32}$$

where

$$\kappa = \sqrt{4\beta_o + \alpha^2 + 8} \tag{33}$$

Hence the four eigenvalues of the transfer matrix are:

$$\lambda_1, \lambda_1^{-1} = -\frac{1}{4}\left[\alpha - \kappa \pm \sqrt{(\alpha-\kappa)^2 - 16}\right] \tag{34}$$

$$\lambda_2, \lambda_2^{-1} = -\frac{1}{4}\left[\alpha + \kappa \pm \sqrt{(\alpha+\kappa)^2 - 16}\right]. \tag{35}$$

To an eigenvalue λ corresponds the eigenvector $[1, \lambda^{-1}, \lambda^{-2}, \lambda^{-3}]^T$. The eigenvectors are arranged **as** columns of the matrix **X,** yielding the transformation

$$\begin{bmatrix} q_i \\ q_{i-1} \\ q_{i-2} \\ q_{i-3} \end{bmatrix} = \begin{bmatrix} 1 & 1 & 1 & 1 \\ \lambda_1^{-1} & \lambda_2^{-1} & \lambda_1^1 & \lambda_2^1 \\ \lambda_1^{-2} & \lambda_2^{-2} & \lambda_1^2 & \lambda_2^2 \\ \lambda_1^{-3} & \lambda_2^{-3} & \lambda_1^3 & \lambda_2^3 \end{bmatrix} \begin{bmatrix} L_1 \\ L_2 \\ R_1 \\ R_2 \end{bmatrix}_i = X \begin{bmatrix} L_1 \\ L_2 \\ R_1 \\ R_2 \end{bmatrix}_i \tag{36}$$

The wave transfer matrix for the system is

$$\begin{bmatrix} L_1 \\ L_2 \\ R_1 \\ R_2 \end{bmatrix}_{i+1} = \begin{bmatrix} \lambda_1 & \lambda_2 & 0 & 0 \\ 0 & 0 & \lambda_1^{-1} & 0 \\ 0 & 0 & 0 & \lambda_2^{-2} \end{bmatrix} \begin{bmatrix} L_1 \\ L_2 \\ R_1 \\ R_2 \end{bmatrix}_i \tag{37}$$

For this hi-coupled assembly there are two pairs of left- and right-traveling waves. For the study of the structure of the passbands, stopbands and complexbands of the system we note that κ is either pure imaginary or real positive. Furthermore, we assume that a is positive. If a is negative, the role of the wavetypes L_1, R_1 and L_2, R_2 is reversed.

For waves L_1,R_1,L_2 and R_2

- $4\beta_o + \alpha^2 + 8 < 0$: In this case κ is imaginary and the operand of the square root in Eqs. **(34)** and **(35)** is complex. These frequencies define a *complexband.*

For waves L_1 and R_1

- $|\alpha - \kappa| < 4$: These frequency ranges define passbands for waves L_1 and R_1. The dispersion relation is:

$$\cos\sigma_1 = -\frac{\alpha-\kappa}{4} \tag{38}$$

- $|\alpha - \kappa| > 4$: These frequency ranges define stopbands for waves L_1 and R_1.
- $|\alpha - \kappa| = 4$: These frequency values define *passband/stopband* edges for waves L_1 and R_1.

For waves L_2 and R_2

- $|\alpha + \kappa| < 4$: These frequency ranges define passbands for waves L_2 and R_2 with the dispersion relation:

$$\cos\sigma_2 = -\frac{\alpha+\kappa}{4} \tag{39}$$

- $|\alpha+\kappa| > 4$: These frequency ranges define stopbands for waves L_2 and *R2.*
- $|\alpha+\kappa| = 4$: These frequency values define *passband/stopband* edges for waves L_2 and *R2.*

It is noteworthy in Eq. **(38)** that since κ is positive, from Eq. **(39),** if $a > 4$ there **is** no passband for the R_2 and L_2 pair.

Example

Figures 8 shows the interblade phase angles and rates of exponential decay for the bi-coupled system in Fig. **4** with A = 1., $\bar{k}_d = 1$ and $\bar{k}_{c1} = k_{c2} = 1$. *The* passband, stopband and complexband structure of the assembly's two characteristic wave pairs is revealed. For this choice of parameters, each wave pair features two separate passbands ($\gamma = 0$), as expected for a two-degree of freedom per site system. Each passband for waves L_2 and R_2 is contained within the corresponding passband for waves L_1 and R_1 and the right passband edges are common to the two wave pairs.

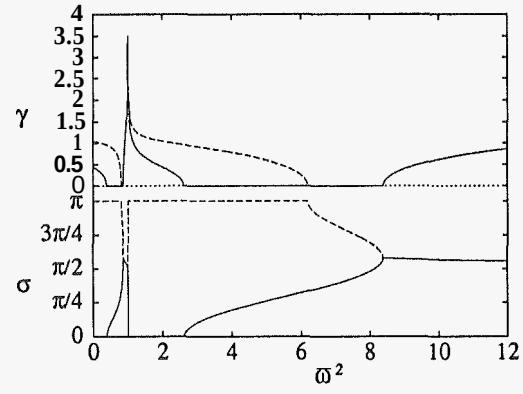

Fig. 8(a) Propagation constants versus frequency for the system in Fig. 4 with $\bar{m} = 1.$, $\bar{k}_d = 1$ and $\bar{k}_{c1} = \bar{k}_{c2} = 1.$ Wave type one is (———) and type two is (– – – –).

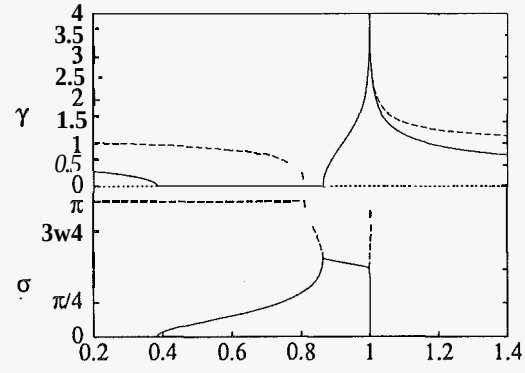

Fig. 8(b) A detailed view of the fir
Wave type one is (———) and – –

As in the mono-coupled system we observe infinite attenuation at $\bar{\omega} = 1$, which corresponds to the natural frequency of the cantilevered blade. Also evident are two complexbands, *i.e.*, frequency ranges where there exist waves with both attenuation and phase shift, As predicted, the two pairs of waves behave as one in the complexbands.

In Fig. 8 the two frequencies at which the transition from passband to complexband occurs are of special importance. At complexband edges $\kappa = 0$, as it goes from pure imaginary to positive real. We noted above that in the passband for wavetype two, $|\alpha + \kappa| < 4$. Hence wavetype two has passbands if and only if $\alpha < 4$. This dramatic change as α goes throught the values 4 is illustrated in Fig. 9.

Figure 9 depicts the propagation constants for the bi-coupled system with $\alpha = \bar{k}_{c1}/\bar{k}_{c2} = 5$. As predicted by Eq. (39), the passband for the L_2, R_2 wave pair has vanished and only stopbands and complexbands remain. The first wave pair still features two distinct passbands in which the interblade phase angle now changes from $\sigma = 0$ at the lower passband edge to $\sigma = \pi$ at the upper passband edge. Motions with all blades vibrating in phase ($\sigma = 0$) and alternate blades vibrating in phase ($\sigma = \pi$) do not stretch the spring k_{c2}, hence the passband edges are uneffected by k_{c2} when $\alpha > 4$.

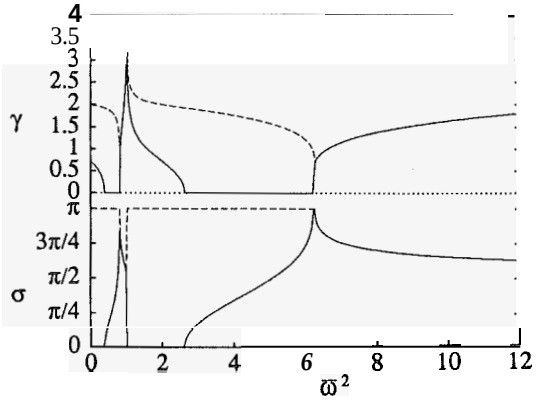

Fig. 9(a) Propagation constants versus frequency for the system in Fig. 4 with $\bar{m} = 1$, $\bar{k}_d = 1$, $\bar{k}_{c1} = 1$ and $k_{c2} = 0.2$. Wave type one is (————) and type two is (– – – –).

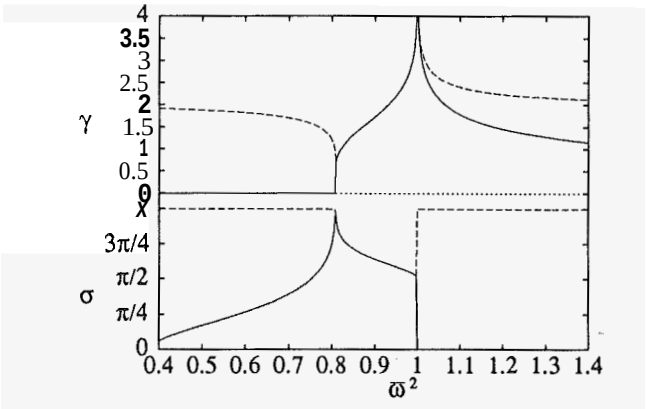

Fig. 9(b) A detailed view of the first passband of Fig. 9(a). Wave type one is (————) and type two is (– – – –).

4 NATURAL FREQUENCIES AND MODE SHAPES OF TUNED CYCLIC STRUCTURES

We search for the natural frequencies of a tuned assembly whose dynamics are described by Eq. (2). Using the cyclic nature of the N-bay system we obtain

$$\mathbf{u}_1 = \mathbf{u}_{N+1} = \boldsymbol{T}_o^N \mathbf{u}_1 \tag{40}$$

where $\boldsymbol{T}_o$ is the transfer matrix for a tuned bay. Hence nontrivial solutions are obtained if and only if

$$\det\left(\boldsymbol{T}_o^N - \boldsymbol{I}\right) = 0. \tag{41}$$

which after some algebra yields the frequency equations

$$\lambda_i(\omega) = \sqrt[N]{1} = e^{j2\pi(n-1)/N} \qquad n = 1, \ldots, N, \tag{42}$$

where λ_i are the eigenvalues of $\boldsymbol{T}_o$. For each value of n the number of frequency solutions to Eq. (42) equals the degrees of freedom in each bay. The complex mode shapes which correspond to these natural frequencies can be found simply through a recursive application of the wave modes given in Section 3. Each mode shape thus features a constant interblade phase angle throughout the assembly. For an N-bay assembly the interblade phase angle can take the following discrete values:

$$\sigma_n = \frac{2\pi(n-1)}{N}, \qquad n = 1, \ldots, N. \tag{43}$$

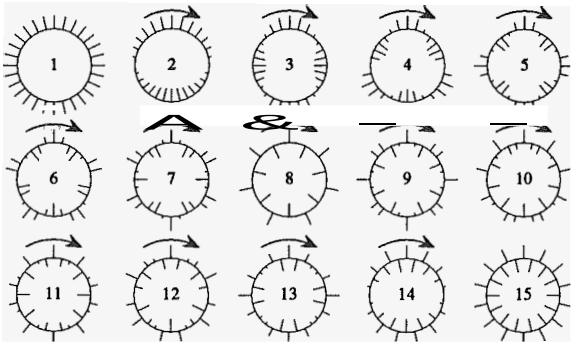

Fig. 10 The global mode shapes of a 28-bay cyclic assembly (system in Fig. 2). The lengths of the radial lines represent the blade displacement amplitudes at an instant of time and the arrows represent the direction of travel for complex modes. The 1st mode is a unique zero nodal diameter ($\sigma_1 = 0$) mode. The 2nd mode is a one nodal diameter ($\sigma_2 = \frac{\pi}{14}$) mode. The 28th mode (not shown) also has one nodal diameter but with $\sigma_{28} = -\frac{\pi}{14}$. The 15th mode is a fourteen nodal diameter ($\sigma_{15} = \pi$) mode and is unique.

Typical constant interblade phase angle mode shapes are depicted in Fig. 10. These modes can also be identified by their number of *nodal diameters,* which are diameters connecting pairs of nodes or bays with zero deflection positioned on opposite sides of the structure. The number of nodal diameters of a mode is directly related

to the interblade phase angle, σ, through Eq. *(43)*. A distinction must be made between the cases of an odd and an even number of blades. If N is odd then for $1 \le n \le (N+1)/2$, the number of nodal diameters equals $(n-1)$ and for $(N+3)/2 \le n \le N$ the number of nodal diameters is $N+1-n$. If N is even, then for $1 \le n \le (N+2)/2$, the number of nodal diameters equals $(n-1)$ and for $(N+4)/2 \le n \le N$ the number of nodal diameters is $N+1-n$. Due to this relationship, the number of nodal diameters and the interblade phase angle may be used interchangeably.

4.1 The Mono-Coupled Assembly

From Eqs. (27) and (42), one obtains

$$\frac{\beta_o(\bar{\omega}_n^p)}{2} \pm \sqrt{\left(\frac{\beta_o(\bar{\omega}_n^p)}{2}\right)^2 - 1} = e^{j2\pi(n-1)/N} \qquad \begin{matrix} n = 1,\ldots,N \\ p = 1,\ldots,P \end{matrix}, \tag{44}$$

where N is the number of blades and P is the number of degrees of freedom per blade. This simplifies as

$$\beta_o(\bar{\omega}_n^p) = 2\cos\sigma_n \qquad \begin{matrix} n = 1,\ldots,N \\ p = 1,\ldots,P, \end{matrix} \tag{45}$$

yielding P natural frequency solutions for each value of the interblade phase angle, hence $N \times P$ natural frequencies for the assembly. From Eq. **(45)** one can easily show that all natural frequencies are double, except those corresponding to $\sigma_1 = 0$ and, if N is even, those corresponding to $\sigma_{(N+2)/2} = \pi$. *Also,* Eq. *(45)* indicates that $-2 \le \beta_o \le 2$, hence the natural frequencies belong to the assembly's passbands (see Eq. (30)), with N frequencies for each of the P passbands.

Example

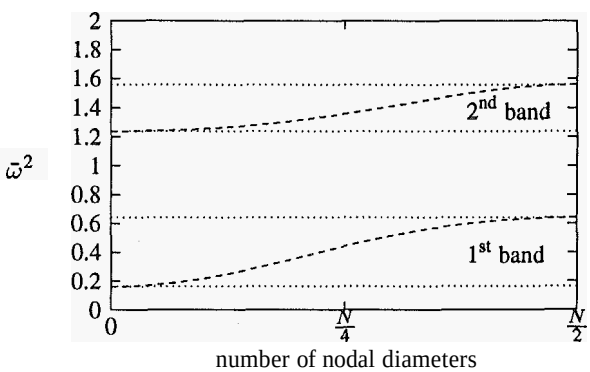

Fig. 11 Natural frequencies as a function of the number of nodal diameters, for both passbands of the system in Fig. 2 with $\bar{k}_c = \bar{k}_d = 1$ and $\bar{m} = 5$.

Turning our attention to the system of Fig. *2*, we have, from Eqs. *(45)* and *(14)*

$$\beta(\bar{\omega}_n) = 2 + \frac{\bar{k}_d}{\bar{k}_c} - \frac{\bar{\omega}_n^2}{\bar{k}_c(1-\bar{\omega}_n^2)} - \frac{\bar{m}\bar{\omega}_n^2}{\bar{k}_c} = 2\cos\sigma_n, \tag{46}$$

which when solved for $\bar{\omega}_n^2$ yields

$$\bar{\omega}_n^2 = \frac{\bar{m} + K(n) + 1 \pm \sqrt{(\bar{m}+K(n)+1)^2 - 4\bar{m}K(n)}}{2\bar{m}} \tag{47}$$

where the minus sign yields values in the first passband and the plus sign gives second passband frequencies. In Eq. (47), $K(n)$ denotes the associated modal stiffness of the disk

$$K(n) = \bar{k}_d + 2\bar{k}_c(1-\cos\sigma_n) \tag{48}$$

where σ_n is the interblade phase angle of the nth mode in each of the passbands, given in Eq. *(43)*. $K(n)$ increases from k_d to $k_d + 4k_c$ as the interblade phase angle varies from 0 to π.

It is customary to plot the natural frequency distribution against the number of nodal diameters. This gives an indication of the number of natural frequencies per unit frequency, *the modal density,* in a given frequency range. In Figure 11 this is done for $\bar{m} = 5$, $\bar{k}_d = 1$ and $k_c = 1$. An interesting feature, sometimes overlooked, is that the curves have local extrema at zero and $N/2$, hence the modal density is greatest at passband edges. The natural frequencies increase monotonically as the number of nodal diameters increases from 0 to $N/2$ and possess no other extrema.

It should also be noted that the natural frequency function of nodal diameters is the inverse of the interblade phase angle function of frequency illustrated in Fig. *7*.

4.2 The Bi-Coupled Assembly

Equations (42), *(34)* and *(35)* yield the set of frequency equations

$$\begin{aligned} -\frac{1}{4}\left[\alpha - \kappa \pm \sqrt{(\alpha-\kappa)^2 - 16}\right] &= e^{j2\pi(n-1)/N} \\ -\frac{1}{4}\left[\alpha + \kappa \pm \sqrt{(\alpha+\kappa)^2 - 16}\right] &= e^{j2\pi(n-1)/N} \end{aligned} \qquad n = 1,\ldots,N. \tag{49}$$

or

$$-\frac{\alpha(\bar{\omega}) - \kappa(\bar{\omega})}{4} = \cos\sigma_n \tag{50}$$

$$-\frac{\alpha(\bar{\omega}) + \kappa(\bar{\omega})}{4} = \cos\sigma_n \tag{51}$$

with σ_n given by *(43)*. Equations (50) and (51) will yield a total of $N \times P$ natural frequencies corresponding modes of type (L_1, R_1) and (L_2, R_2) respectively.

Example

Solving Eqs. (50) and (51) for the system in Fig. *4* yields

$$\bar{\omega}_n^2 = \frac{\bar{m} + K(n) + 1 \pm \sqrt{(\bar{m}+K(n)+1)^2 - 4\bar{m}K(n)}}{2\bar{m}} \tag{52}$$

where

$$K(n) = \bar{k}_d + 2\bar{k}_{c1}(1-\cos\sigma_n) + 2\bar{k}_{c2}(1-\cos 2\sigma_n), \tag{53}$$

is the modal stiffness of the disk for the modes of interblade phase angle σ_n. Note that the expressions of the natural frequencies of the mono-coupled system, Eqs. *(47)* and (48), and of the bi-coupled system, Eqs. (52) and (53), are similar, except for the modal disk stiffness, $K(n)$, which is modified by the additional coupling spring. As was the case with the mono-coupled system (Eq. (48)), $K(n)$ has values k_d and $k_d + 4k_c$ at the interblade phase angles 0 and π, respectively. The effect of k_{c2} on $K(n)$ occurs

only between $\sigma = 0$ and $\sigma = \pi$ and is largest for $\sigma = \pi/2$. The consequence is that whereas the natural frequencies of the mono-coupled system increase monotonically, we find that Eq. (52) may possess a maximum at an interblade phase angle given by

$$\cos\sigma = -\frac{k_{c1}}{4k_{c2}} \tag{54}$$

which has no solution when $a = k_{c1}/k_{c2} > 4$. Recall that the frequency function in Eq. (52) is the inverse of the dispersion relation in the passbands plotted in Figs. 8 and 9. The maximum of Eq. (52) thus corresponds to the frequency of transition from passband to complexband in Figs. 8 and 9. The location of the maximum varies from $\sigma = \pi$ to $\frac{\sigma=\pi}{2}$ as $\alpha = \frac{k_{c1}}{k_{c2}}$ varies from 4 to zero. Its occurrance as a becomes smaller than 4 signifies the birth of passbands for the second wave type, as discussed in section 3.2.

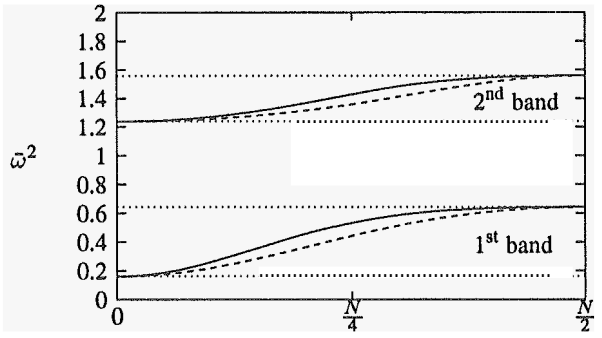

Fig. 12 Natural frequencies as a function of the number of nodal diameters, for both passbands of the system in Fig. 4 with $\bar{m} = 5$, $\bar{k}_d = \bar{k}_{c1} = 1$ and $\bar{k}_{c2} = 0.2$ (———)The natural frequency curve for the mono-coupled system with $\bar{m} = 5$, $\bar{k}_d = \bar{k}_c = 1$ (— — — —)is shown for comparison. Passband edges are denoted by (·····).

Figure 12 displays the natural frequencies in both passbands as a function of the number of nodal diameters for $k_{c1} = 1$ and $k_{c2} = 0.2$, *i.e.*, the coupling between nearest neighbors is five times stronger then the coupling between bays that are separated by one bay ($a = 5$). In this case there are no passbands for the second wave type (see Eq. (39) and Fig. 9) and thus all normal modes are associated with the first wave type. Furthermore, since for $a = 5$ the passband edges occur for $\sigma = 0$ and π (see Fig. 9) and since the corresponding natural frequencies are independent of the non-adjacent coupling stiffness, k_{c2} (see Eq. (53)), the bi-coupled system and the mono-coupled assembly feature the same frequency passbands, as depicted in Fig. 12. Note, however, that the variation of the natural frequencies with the interblade phase angle, or the number of nodal diameters, is different for the mono- and bi-coupled systems, though it is monotonous in both cases. In particular, the modal density of the bi-coupled system is larger for the higher numbers of nodal diameters.

Figure 13 shows the natural frequencies in both passbands as a function of the number of nodal diameters for $\bar{k}_{c1} = 1$ and $\bar{k}_{c2} = 1$, hence $a = 1$. Since k_{c2} is greater than $k_{c1}/4$, Eqs. (38) and (39) indicate that passbands must exist for both wave types. Indeed, we observe in Fig. 13 the widening of the passbands for the type-one wave and the appearance of passbands for the second wave type (this can also be seen in Fig. 8). Apparent in Fig. 13 is the non-monotonous variation of the natural frequencies with the number of nodal diameters, as predicted by Eq. (54). The maxima shown in Fig. 13— one for each passband — would occur for all values of $\alpha < 4$. On each frequency curve, the maximum separates the normal modes that are associated with each type of wave: the modes that feature a number of nodal diameters (or an interblade phase angle) that is smaller than that of the maximum belong to the first wave type, while those whose interblade phase angle is larger than that of the maximum are associated with the second wave type. This is also evidenced in Fig. 8. Clearly the number of free vibration modes associated with the second wave type increases with the stiffness k_{c2}. From Eq. (54)it may be seen that as $k_{c2} \to \infty$, the location of the peak frequency goes to $\sigma = \pi/2$ ($n = N/4$), at which point the number of modes of type 1 equals (approximately) that of type 2.

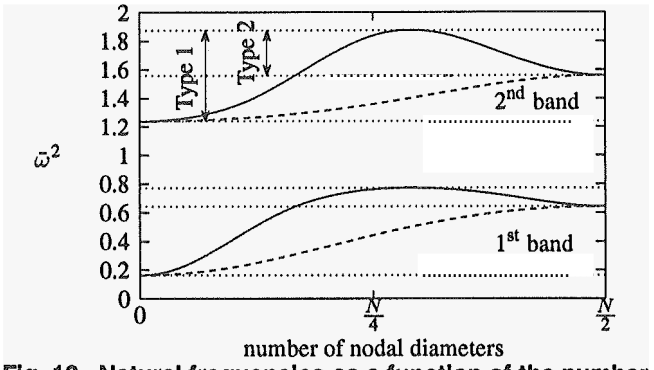

Fig. 13 Natural frequencies as a function of the number of nodal diameters, for both passbands of the system in Fig. 4 with $\bar{m} = 5$ and $\bar{k}_d = \bar{k}_{c1} = \bar{k}_{c2} = 1$ (———)The natural frequency curve for the mono-coupled system with $\bar{m} = 5$, $\bar{k}_d = \bar{k}_c = 1$ (— — — —)is shown for comparison. Passband edges for the two wave types are denoted by (·····).

It is important to note that when k_{c2} becomes greater than $k_{c1}/4$, that is, when the non-adjacent coupling spring stiffness becomes sufficiently large, the dynamic characteristics of the bi-coupled system become qualitatively different from those of the mono-coupled assembly. In these cases the adjacent coupling assumption may not be valid.

5 WAVES AND MODES IN MISTUNED CYCLIC STRUCTURES

As an example of the effect of random mistuning, we consider the mode shapes of the mistuned blade assembly model depicted in Fig. 2. Figure 14 displays some of the mode shapes in the second frequency cluster of a 28-blade assembly. The modes have changed drastically compared to the tuned modes depicted in Fig. 10. High levels of localization are observed, such that the vibrational energy of a localized mode shape is no longer uniformly distributed along the rotor, but is concentrated in a handful of blades (as few as five) that feature significantly larger amplitudes than the majority of blades. Such mode localization may result in a substantial increase in free response amplitudes and in a potential decrease in fatigue life.

In order to achieve a compact characterization of localization phenomena, a stochastic approach is chosen to analyze the effects of random blade mistuning. The statistical description is not well suited to the modes of vibration because of the switching of the

associated natural frequencies as the strength or the distribution of mistuning varies. We choose instead to examine the frequency-dependent propagation of incident waves in mistuned assemblies.

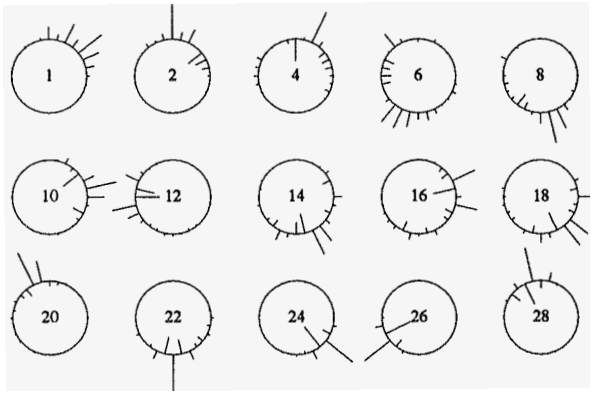

Fig. 14 Localized modes in the second frequency cluster of a 28 blade assembly with $\bar{k}_d = \bar{m} = 1$, $\bar{k}_c = 0.1$, and uniform random mistuning in the blade stiffness with 5% standard deviation ($s_b = 0.05$). The lengths of the radial lines represent the blade displacement amplitudes. Modes are sorted by increasing natural frequency.

In order to avoid the contamination of the localization effect by the cyclicity condition, an infinite assembly is studied, which consists of a segment of N mistuned bays ($i = 1, \ldots, N$) embedded in an otherwise tuned infinite assembly. Our interest lies in the transmission of incident waves along the N-bay mistuned segment. An advantage of this setup is that a wave that exits the mistuned segment is propagated away and does not return. We then let N go to infinity in order to obtain an asymptotic characterization of wave transmission through mistuned bays.

For tuned systems, characteristic waves propagate independently of one another and, in frequency passbands, are unattenuated. Mathematically this is expressed by the fact that for a tuned bay the transformation from physical to wave coordinates renders the wave transfer matrix diagonal (see Section 3). For a mistuned bay, however, the transformation defined by $\mathbf{X}$ does not, in general, diagonalize the random bay transfer matrix, $\boldsymbol{T}_i$. This means that a wave incident to a mistuned segment is not fully transmitted along the segment, but rather experiences scattering at each interface between dissimilar bays, giving rise to reflected and transmitted components in all the characteristic wave types for the assembly. The effect of these multiple reflections over a number of mistuned bays is to trap the incident wave near the incidence region—this is the phenomenon referred to as ***localization*** (Kissel, 1988). *Also*, the conversion of the incident wave into the other wave types may cause the transmitted wave which exits the mistuned segment to be quite different, in terms of amplitude but also of wave type components, from the incident wave—a phenomenon referred to as ***wave conversion*** (Chen and Pierre, 1992). The mathematical formalism used in the study of localization and conversion phenomena follows.

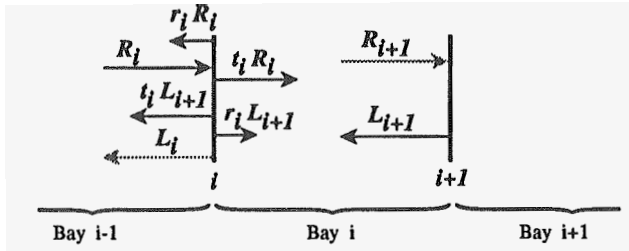

Fig. 15 Scattering of waves at substructure interfaces

At the interface between dissimilar bays, waves are split into transmitted part and reflected components. As illustrated in Fig. 15, the left-going wave vector incident to bay $(i-1)$, $\mathbf{L}_i$, is the sum of transmitted left-going waves, $\mathbf{t}_i\mathbf{L}_{i+1}$, and reflected right-going waves, $\mathbf{r}_i\mathbf{R}_i$. Likewise, $\mathbf{R}_{i+1}$ is comprised of a transmitted wave vector, $\mathbf{t}_i\mathbf{R}_i$, and a reflected wave vector, $\mathbf{r}_i\mathbf{L}_{i+1}$. Here $\mathbf{t}_i$ and $\mathbf{r}_i$ are the (complex) transmission and reflection matrices for the ith bay, where directional symmetry has been assumed. This leads to the general form of the wave transfer matrix:

$$\begin{bmatrix} \mathbf{L} \\ \mathbf{R} \end{bmatrix}_{i+1} = \mathbf{W}_i \begin{bmatrix} \mathbf{L} \\ \mathbf{R} \end{bmatrix}_i = \begin{bmatrix} \mathbf{t}_i^{-1} & -\mathbf{t}_i^{-1}\mathbf{r}_i \\ \mathbf{r}_i\mathbf{t}_i^{-1} & \mathbf{t}_i - \mathbf{r}_i\mathbf{t}_i^{-1}\mathbf{r}_i \end{bmatrix} \begin{bmatrix} \mathbf{L} \\ \mathbf{R} \end{bmatrix}_i . \quad (55)$$

Equation *(55)* tells us that the off-diagonal blocks in $\mathbf{W}_i$ govern what portion of a left- or right-traveling wave vector is being reflected. The transmitted portion of the incident wave vector is determined by the first diagonal block in the wave transfer matrix. For a tuned bay, $\mathbf{W}_i \equiv \mathbf{W}_o$ is diagonal and its elements are the eigenvalues of the transfer matrix $\mathbf{T}_o$, hence there are no reflections and no conversions of a given wave type into the other types. Hence $\mathbf{r}_i = 0$ and $\mathbf{t}_i$ is diagonal and equal to $\boldsymbol{\Lambda}^{-1}$ from Eq. *(26)*. For a mistuned bay there are reflections as well as transmissions of a given incident wave type into all wave types, leading to wave localization and conversion phenomena. Hence passbands no longer exist and all waves are attenuated for all frequencies. The off-diagonal elements of $\mathbf{r}_i$ and $\mathbf{t}_i$ govern the converted components of the reflected and transmitted portions of the incident wave vector, respectively.

For a segment of N dissimilar bays the wave transfer matrix is the product of the random wave transfer matrices of the individual bays:

$$\mathcal{W}_N = \prod_{i=1}^{M} \mathbf{W}_i = \begin{bmatrix} \tau_N^{-1} & -\tau_N^{-1}\rho_N \\ \rho_N\tau_N^{-1} & \tau_N - \rho_N\tau_N^{-1}\rho_N \end{bmatrix} . \quad (56)$$

where τ_N and ρ_N are the transmission and reflection coefficient matrices for the mistuned segment. The first diagonal block of $\mathcal{W}_N$ tells us which portion of an incident wave vector is being transmitted to the far end of the mistuned segment. Hence the behavior of the transmission coefficient matrix, τ_N, governs the strength of the effects of mistuning and the resulting wave localization and conversion. Asymptotically, the "long-term" spatial behavior of τ_N can be characterized by the ***localization factors***

$$\gamma_j = -\lim_{N\to\infty} \frac{1}{N} \ln \sigma_j(\tau_N) \qquad j = 1, \ldots, M \quad (57)$$

where M is the number of coupling coordinates for the system and thus the number of wave types and σ_j is the jth singular value of the transmission matrix τ_N, that is, the positive square root of the jth eigenvalue of $\tau_N^H\tau_N$, where H denotes a complex conjugate transpose. Equation (57) means that asymptotically, the singular values of τ_N decrease exponentially with N at the rates per bay

$-\gamma_j, j = 1, \ldots, M$. The M localization factors may be thought of as being associated with the M different wave types and characterize the amplitude decay of wave vectors. The localization factors can be shown to be the positive lyapunov exponents of the product of the random wave transfer matrices, $\mathbf{W}_i$ (Kissel, 1988).

Although the localization factors defined in Eq. (57) provide a compact characterization of the exponential decay of wave vectors and thus of localization of the various wave types due to mistuning, at the present time, there are no known theoretical tools to develop approximations of them in the multi-coupled case. This is essentially due to the complex interactions that take place among the various wave types. Obviously closed-form solutions cannot be obtained either, and one would have to resort to a purely numerical evaluation of the γ_j's, for example using an algorithm for the calculation of Lyapunov exponents, which is beyond the scope of this work. Approximations of the localization factors are, however, available in the mono-coupled case (Pierre, 1990). Below we first summarize these results and then examine under which conditions they are applicable to bi-coupled systems (for which the localization factors are not available) by making use of our insights into the influence of an additional coupling coordinate on the passband structure of the tuned assembly.

5.1 Mono-coupled assembly

For a mono-coupled assembly there is only one coupling coordinate and one pair of waves, and the transmission coefficient, τ_N, is a scalar. Hence there exists a single localization factor, obtained from Eq. (57) for $M = 1$:

$$\gamma = -\lim_{N\to\infty} \frac{1}{N} \ln|\tau_N|, \tag{58}$$

implying that asymptotically, the ratio of emergent to incident wave amplitude decreases exponentially with an increasing number of bays, N (Pierre, 1990). At this point it is noteworthy that the assumption that the structure is infinite is a limitation. This type of analysis is only applicable if localization is strong enough that the vibration energy is confined to region which is small compared to assembly size. For a cyclic system this requires that the wave be adequately attenuated before reaching the incidence region again and thus interacting with other waves from the same source.

In general Eq. (58) for the localization factor cannot be evaluated in closed form. However, analytical approximations are possible using perturbation methods in this mono-coupled case. These are derived in detail in (Óttarsson and Pierre, 1993) and the main results are outlined below.

We seek an expansion of τ_N in Eq. (58) in terms of the small mistuning parameter, thus treating the mistuned system as a perturbation of the tuned system. This is obtained through a Taylor series expansion of the function $\beta(\delta_i)$ in Eq. (5):

$$\beta(\delta_i) = \beta_o + \beta'(0)\delta_i + O(\delta_i^2) \tag{59}$$

and subsequent expansions of the transfer matrix Ti, of the wave transfer matrix product $\mathcal{W}_N$, and of τ_N. Finally, expanding the expression of γ, Eq. (58), to the first-order in the variance of the mistuning and taking the limit yields:

$$\gamma \simeq \frac{1}{2}\left(\frac{\beta'(0)s_\delta}{2\sin\sigma}\right)^2 = \frac{\beta'(0)^2 s_\delta^2}{2(2+\beta_o(\bar{\omega}))(2-\beta_o(\bar{\omega}))} \tag{60}$$

In the calculation the random variables δ_i were considered independent and identically distributed, with zero mean and standard deviation s_δ. Also note that this analysis is limited to the tuned system's passbands, since there is already large attenuation in the stopband.

In Eq. (60), both β_o and $\beta'(0)$ are functions of Ω and vary within each passband. The onset of localization is observed to increase with the square of the mistuning standard deviation and also with the square of $\beta'(0)$. (In (Óttarsson and Pierre, 1993), $\beta'(0)$ was defined as the sensitivity measure for the mono-coupled assembly—see below.) Furthermore, the approximation of the localization factor becomes unbounded at frequencies which correspond to the edges of the passbands of the tuned assembly, $\beta_o = \pm 2$. This is reasonable, since at those frequencies the transformation matrix X (see Eq. (28)) is singular.

In order for Eq. (60) to be valid, the expansion in Eq. (59) must of course be uniform, *i.e.*, $\beta'(0)$ must be of order one (order ϵ^0) or smaller. However, if the expansion is nonuniform, *i.e.*, when $\beta'(0)$ is large (order ϵ^{-1} or larger) the technique breaks down. In this case the perturbation expansion is only valid for δ_i second-order (order ϵ^2) or smaller. This may also be seen by the fact that γ in Eq. (60) becomes large for $\beta'(0)$ large, while it supposedly is a small perturbation of its zero value in the tuned system's passbands. This breakdown indicates high sensitivity to mistuning and it is when the breakdown occurs (if it occurs) that systems have been seen to enter the realm of strong localization. This suggests the use of the first-order Taylor coefficient of $\beta(\delta_i)$ as a *measure of sensitivity to mistuning* for the mono-coupled system, which has been explored thoroughly in (Óttarsson and Pierre, 1993).

When the sensitivity measure, $S = \beta'(0)$, other avenues must be explored to capture the qualitative changes in the assembly's dynamics. Note that in the passbands of the tuned system we have $-2 \le \beta_o \le 2$, but when S is large, $\beta(\delta_i)$ in Eq. (59) has the potential to become large for first-order mistuning in that frequency range. This suggests treating the off-diagonal terms in the transfer matrix of Eq. (5) as small perturbations compared to the large $\beta(\delta_i)$, thus yielding the following alternative expansion for the high sensitivity case:

$$\boldsymbol{T}_i = \begin{bmatrix} \beta(\delta_i) & -1 \\ 1 & 0 \end{bmatrix} = \begin{bmatrix} \beta(\delta_i) & 0 \\ 0 & 0 \end{bmatrix} + \begin{bmatrix} 0 & -1 \\ 1 & 0 \end{bmatrix} = \bar{\boldsymbol{T}}_i + \boldsymbol{T}_\epsilon. \tag{61}$$

A brief review of the equation of motion, Eq. (4), aids in a physical interpretation of Eq. (61). The larger β becomes compared to 1, the less q_i is influenced by q_{i+1} and q_{i-1}. Consequently, in Eq. (61), a coupled system is treated as a perturbation of the uncoupled system. Since the modified unperturbed matrix $\bar{\boldsymbol{T}}_i$ is already diagonal, there is no need for a wave coordinate transformation, and it is easily shown that the localization factor can be approximated as, in this case of high sensitivity to mistuning:

$$\gamma = \langle \ln|\beta(\delta)| \rangle = \int \ln|\beta(\delta)| \mathrm{pdf}_\delta(\delta) d\delta, \tag{62}$$

where $\langle\rangle$ denotes an average and $\mathrm{pdf}_\delta(\delta)$ is the probability density function of the random variable δ.

The two approximations of the localization factor, Eqs. (60) and (62), allow for the onset of localization and strong localization behavior, respectively, to be characterized in a simple and compact way, without extensive simulations of mistuned systems. Note that Eqs. (60) and (62) are general and apply to any mono-coupled mistuned assembly.

Example

From Eqs. (12), (60) and (62), we calculate for the system in Fig. 2 the localization factor approximations in cases of low and high sensitivity. These are found to be:

Weak Sensitivity

$$\gamma \simeq \frac{1}{\bar{k}_c^2}\left[\frac{\bar{\omega}^2}{(1-\bar{\omega}^2)}\right]^4 \frac{s_b^2}{8\sin^2\sigma} \tag{63}$$

where s_b is the standard deviation of the random blade frequency mistuning.

Strong Sensitivity

$$\gamma \simeq \frac{(1-\bar{\omega}^2)\beta_o \ln\left|\frac{\beta(\sqrt{3}s_b)}{\beta(-\sqrt{3}s_b)}\right|}{2\sqrt{3}s_b\left(\beta_o + \frac{\bar{\omega}^4}{\bar{k}_c(1-\bar{\omega}^2)}\right)} + \frac{\ln\left|\beta(\sqrt{3}s_b)\beta(-\sqrt{3}s_b)\right|}{2} - \frac{\bar{\omega}^4 \ln\left|\frac{1-\bar{\omega}^2+\sqrt{3}s_b}{1-\bar{\omega}^2-\sqrt{3}s_b}\right|}{2\bar{k}_c\sqrt{3}s_b\left(\beta_o + \frac{\bar{\omega}^4}{\bar{k}_c(1-\bar{\omega}^2)}\right)} \tag{64}$$

Verification of the localization factor approximations is performed by Monte Carlo simulations and consists of two parts. On the one hand we verify the variation of γ as a function of frequency by running a series of simulations for a range of frequencies and plot the results along with the perturbation approximations in the passbands. The other part of the simulation process is the verification of the two perturbation solutions at the mid-passband frequencies as a function of the sensitivity measure, $S = \beta'(0)$. It is clear that both γ_{mid} and S_{mid} are functions of k_c, $\bar{k}_d$ and $\bar{m}$ and may thus be parameterized with any or all of these parameters. This offers the opportunity to examine the ***invariance*** of the relationship between γ_{mid} and S_{mid} with respect to the system parameters and the passband number.

Monte Carlo simulations were performed in the following manner. A series of random transfer matrices representing the bays of a finite, cyclic assembly were generated, based on a random sequence, δ_i, from a random number generator. We labeled the resulting assembly one ***realization*** of mistuning. The matrices were multiplied together and transformed into wave coordinates, yielding the wave transfer matrix for the mistuned assembly (see Eq. (56)). The localization factor for this particular realization of an N-bay system was then calculated from Eq. **(58)** (of course, without taking the limit). This was repeated for a large number of realizations of the assembly and the result averaged, adding realizations until the desired accuracy had been reached. The above constitutes one Monte Carlo simulation, for a system with some set of parameters $\bar{k}_c$, $\bar{k}_d$ and $\bar{m}$ vibrating at some frequency. For the Monte Carlo simulations a uniform distribution of width $2W$ and standard deviation $W/\sqrt{3}$ was assumed for the mistuning.

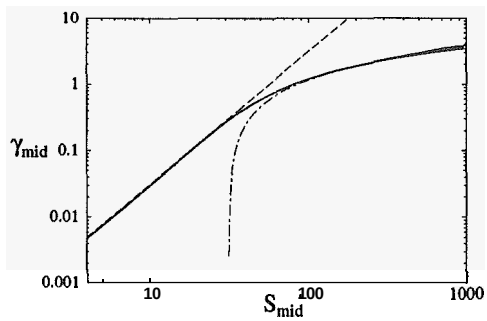

Fig. 16 Monte Carlo simulations (———) are used to verify Eqs. (63) (— — -) and (64) (— · —). Multiple Monte Carlo simulations are obtained by varying $\bar{m}$ in 1st passband, $\bar{k}_d$ in 2nd passband and $\bar{k}_c$ in 1st passband. The standard deviation of blade stiffness mistuning is 5%. Note the near overlap of the various Monte Carlo results.

Figure 16 illustrates the transition from the low-sensitivity perturbation approximation of the mid-band localization factor to the high-sensitivity approximation. The sensitivity measure at midband frequencies, S_{mid}, is affected by all parameters, $\bar{m}$, k_c and $\bar{k}_d$ as well as the passband number. Figure 16 contains three overlapping Monte Carlo simulation curves, each obtained by varying a different system parameter, *i.e.*, $\bar{m}$ in 1st passband, $\bar{k}_d$ in 2nd passband, and finally, k_c in 1st passband. These curves overlap nearly perfectly, except for a slight discrepancy at very high sensitivity). This suggests that $S = \beta'(0)$ is indeed highly suitable as a ***universal*** measure of sensitivity for mono-coupled systems.

Figure 17 shows the localization factor as a function of frequency in a system that has low sensitivity in the second passband but high first passband sensitivity. In the second passband the low-sensitivity solution provides an excellent prediction of weak localization. In the first passband the high-sensitivity solution matches the simulated results, thereby confirming the strong localization approximation.

5.2 The Bi-Coupled Assembly

As stated above, localization factor approximations are not yet obtainable for assemblies with more than one coupling coordinate, hence not permitting an in-depth study of localization in the bi-coupled assembly. In Section 4 we have observed how the introduction of an additional coupling coordinate introduces a second wave channel in the assembly but that it is not until the associated non-adjacent coupling stiffness is sufficiently strong ($a < 4$) that the additional wave channel is capable of energy-carrying motion. This suggests that localization results obtained for mono-coupled mistuned assemblies may be applicable to bi-coupled ones as long as there are no frequency passbands associated with the additional wave type. In the following we attempt to draw qualitative conclusions about the effect of the additional coupling coordinate through the study of the example system in Fig. 4.

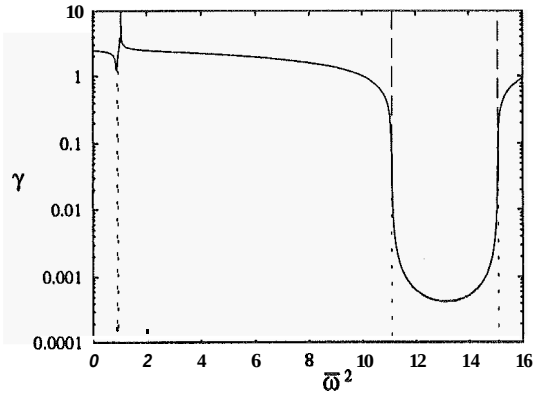

(a) $S_{mid_2} \simeq 1.2$

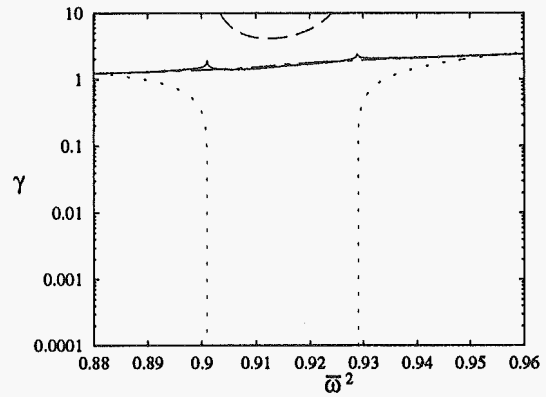

(b) $S_{mid_1} \simeq 123$ (1^{st} passband)

Fig. 17 Exponential decay rate, γ, due to 5% blade stiffness mistuning *vs.* frequency. In stopbands Monte Carlo simulations (———) agree with the propagation constant for the tuned system (·····). In (a) the simulations results overlap the classical perturbation result (— — -), Eq. (63), in the 2^{nd} passband. In (b) the simulation agrees with the modified perturbation result (— · —), Eq. (64).

Example

A study of the natural frequencies of the system in Fig. 4 demonstrated how the introduction of the non-adjacent coupling spring initially causes an increase in modal density at the upper passband edge while not affecting the passband width (see Fig. 12). Increasing k_{c2} (or decreasing a) beyond $k_{c1}/4$ (or below $a = 4$) causes an increase in passband width and a subsequent decrease in modal density, as shown in Fig. 13.

Perturbation methods for the eigenvalue problems have been used previously to predict the effects of mistuning on the free dynamics of periodic structures (Pierre and Cha, 1989; Murthy and Pierre, 1992). Since the second-order eigenvalue perturbations due to mistuning are inversely proportional to the distance between the tuned eigenvalues, it results that the sensitivity to mistuning, and thus localization effects, typically increase as the modal density of the tuned assembly increases. Using this result we make the following predictions about the influence of the non-adjacent coupling spring k_{c2} on the sensitivity to mistuning.

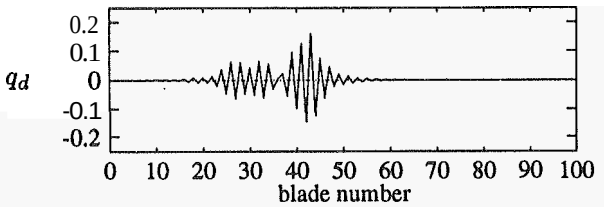

Fig. 18 Mode 98 in a 100-blade mono-coupled assembly with natural frequency $\bar{\omega}^2 = 0.6439$. $\bar{m} = 5$, $\bar{k}_d = 1$ and $\bar{k}_c = 1$. The standard deviation of mistuning is 8%

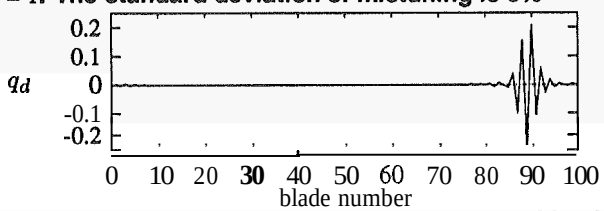

Fig. 19 Mode 92 in a 100-blade bi-coupled assembly with natural frequency $\bar{\omega}^2 = 0.6439$. $\bar{m} = 5$, $\bar{k}_d = 1$, $k_{c1} = 1$ and $k_{c2} = 0.2$. The standard deviation of mistuning is 8%

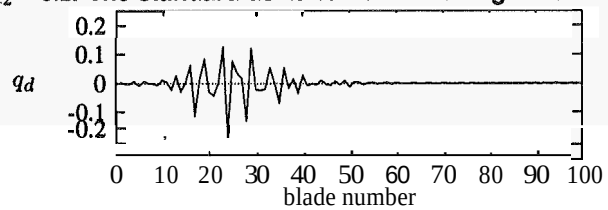

Fig. 20 Mode 73 in a 100-blade bi-coupled assembly with natural frequency $\bar{\omega}^2 = 0.6446$. $\bar{m} = 5$, $\bar{k}_d = 1$, $k_{c1} = 1$ and $k_{c2} = 0.4$. The standard deviation of mistuning is 8%

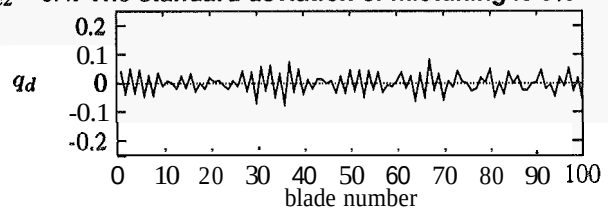

Fig. 21 Mode 40 in a 100-blade bi-coupled assembly with natural frequency $\bar{\omega}^2 = 0.6448$. $\bar{m} = 5$, $\bar{k}_d = 1$, $k_{c1} = 1$ and $k_{c2} = 1$. The standard deviation of mistuning is 8%

- In the range $0 < k_{c2} < k_{c1}/4$, modal density at the upper edge of the passbands (where mistuning sensitivity is the greatest) is increased compared to the mono-coupled system, causing an increase in mistuning sensitivity beyond what is predicted by the mono-coupled analysis, The modal density reaches a maximum when $k_{c1}/k_{c2} = 4$.
- For $k_{c2} > k_{c1}/4$, the modal density in the neighborhood of natural frequency of the $N/2$ interblade phase angle modes (previously the upper passband edge) decreases. *Also,* a widening of the passband occurs with a corresponding decrease in modal density throughout the passband, and a subsequent decrease in sensitivity to mistuning.

Localized modes provide ample evidence of this behavior. As an example, we examine the modes of vibration of a 100-blade mistuned system with $\bar{m} = 5$, $\bar{k}_d = 1$ and $\bar{k}_{c1} = 1$. For a given random mistuning pattern, we follow mode shapes occurring at $\bar{\omega}^2 \simeq 0.644$. as $\bar{k}_{c2}$ is increased from 0 to 1. This frequency is located just below the upper edge of the first passband of the mono-

coupled system and thus corresponds to the maximum localization in the mono-coupled system.

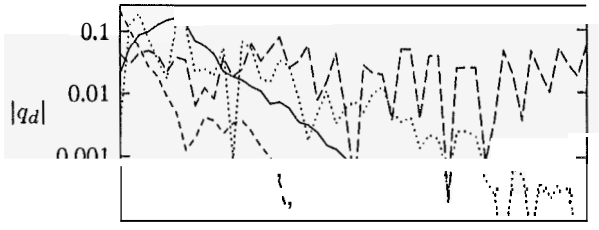

Fig. 22 Comparison of amplitude decay for mistuned modes with natural frequency $\bar{\omega}^2 \simeq 0.644$. The absolute value of the blade displacement is plotted on a logarithmic scale with the mode peaks aligned. Mono-coupled (———), $\alpha = 5$ (– – – –), $\alpha = 2.5$ (·····), $\alpha = 1$ (— — —).

The modes studied are depicted in Figs. 18-21. The localization effect of mistuning is evident for both mono- and bi-coupled systems. Comparing Fig. 18 with Fig. 19, as $\bar{k}_c$ is increased from 0 to 0.2 the increased-modal density causes increased localization. A further increase to $k_{c2} = 0.4$ results in weaker localization, to a strength lower than that of the mono-coupled system. For $\bar{k}_{c2} = 1$, localization at $\bar{\omega}^2 \simeq 0.644$ has all but vanished. A more accurate examination of these four mode shapes is possible by plotting the absolute value of the displacement of each mode on a logarithmic scale and aligning the mode peaks. Figure 22 demonstrates that the behavior of the rate of decay as k_{c2} increases is as outlined above.

6 CONCLUSIONS

The vibrations of mistuned mono- and bi-coupled blade assemblies were studied using a transfer matrix approach. A mono-coupled assembly may be modeled using a 2 x 2 transfer matrix whereas the bi-coupled system requires a 4 x 4 transfer matrix. Throughout the paper the theory was illustrated by example systems for each type of assembly

The theory of wave propagation in multi-coupled periodic structures was reviewed and detailed for the mono- and bi-coupled assemblies. The study identified that if coupling of neighboring blades is more than four times stronger than the coupling of blades separated by one blade, then the wave propagation properties of the mono- and bi-coupled assemblies are qualitatively the same.

A study of the natural frequency distribution of the mono- and bi-coupled assemblies revealed that mistuning sensitivity, as predicted by an analysis of a mistuned mono-coupled system, may initially increase when non-adjacent bay coupling is introduced. Sensitivity was found to reach a maximum when coupling of neighboring blades is four times as strong as the coupling of blades separated by one blade. For higher values of the non-adjacent coupling, mistuning sensitivity was decreased and localization all but vanished when the non-adjacent coupling became as strong as the adjacent coupling. These conclusions were supported by the examination of the localized modes of mistuned bi-coupled systems with various levels of interblade coupling.

7 REFERENCES

- Bendiksen, O. O., 1984, "Flutter of Mistuned Turbomachinery Rotors," *ASME Journal of Engineering for Gas Turbines and Power,* Vol. 106, No. 1, pp. 25–33.
- Brillouin, L., 1953, *Wave Propagation in Periodic Structures,* New York: Dover.
- Chen, W. J. and Pierre, C., 1992, "Vibration Localization and Wave Conversion Phenomenon in a Multi-Coupled, Nearly Periodic Disordered Truss Beam," *AZAA Paper 92-1115, Proceedings of the AIAA Dynamics Specialists Conference, Dallas, Texas,*
- Cornwell, P. J. and Bendiksen, O. O., 1987, "Localization of Vibrations in Large Space Reflectors," *AIAA Journal,* Vol. 27, No. 2, pp. 219–226.
- Davis, P. J., 1979, *Circulant Matrices,* NYC: Wiley-Interscience,
- Dye, R. C. and Henry, T. A., 1969, "Vibration Amplitudes of Compressor Blades Resulting From Scatter in Blade Natural Frequencies," *ASME Journal of Engineering for Power,* Vol. 91, pp. 182–188.
- El-Bayoumy, L. E. and Srinivasan, A. V., 1975, "Influence of Mistuning on Rotor-Blade Vibrations," *AIAA Journal,* Vol. 13, No. 4, pp. 460–464.
- Ewins, D. J. and Han, Z. S. 1984, "Resonant Vibration Levels of a Mistuned Bladed Disk," *ASME Journal of Wbration, Acoustics, Stress and Reliability in Design,* Vol. 106, pp. 211–217.
- Hodges, C. H., 1982, "Confinement of Vibration by Structural Irregularity," *Journal of Sound and Wbration,* Vol. 82, No. 3, pp. 411–424.
- Kissel, G. J., 1988, "Localization in Disordered Periodic Structures." *Ph.D. Dissertation, Massachusetts Institute of Technology.*
- Mead, D. J., 1975, "Wave Propagation and Natural Modes in Periodic Systems, 11: Multi-Coupled Systems, With and Without Damping," *Journal of Sound and Mbration,* Vol. 40, pp. 19–39.
- Murthy, D. V. and Pierre, C., 1992 "Stochastic Sensitivity Measure for Mistuned High-Performance Turbines." *NASA Technical Memorandum 105821.*
- Óttarsson, G. S. and Pierre, C., 1993, "A Transfer Matrix Approach to Vibration Localization in Mistuned Blade Assemblies" *Proceedings of ASME Gas Turbine Conference, Cincinnati.*
- Pierre, C. and Cha, P.D. 1989, "Strong Mode Localization in Nearly Periodic Disordered Structures," *AZAA Journal,* Vol. 27, No. 2, pp. 227–241.
- Pierre, C., 1990, "Weak and strong vibration localization in disordered structures: a statistical investigation," *Journal of Sound and Wbration,* Vol. 139, pp. 111–132.
- Srinivasan, A. V., 1984, "Vibrations of Bladed-Disk Assemblies — A Selected Survey," *ASME Journal of Vibration, Acoustics, Stress and Reliability in Design,* Vol. 106, No. 2, pp. 211–217.
- Valero, N. A. and Bendiksen, O. O., 1986, "Vibration Characteristics of Mistuned Shrouded Blade Assemblies," *ASME Journal of Engineering for Gas Turbines and Power,* Vol. 108, No. 2, pp. 293–299.
- Wei, S. T. and Pierre, C., 1988, "Localization Phenomena in Mistuned Assemblies With Cyclic Symmetry, Part I: Free Vibrations," *ASME Journal of Wbration, Acoustics, Stress and Reliability in Design,* Vol. 110, No. 4, pp. 429–438.